JVSTB Journal of Vacuum Science & Technology B

Probing complex low-dimensional solids with scanning probe microscopes: From charge density waves to high-temperature superconductivity

Jie Liu, Jin-Lin Huang, and Charles M. Lieber

Citation: Journal of Vacuum Science & Technology B **14**, 1064 (1996); doi: 10.1116/1.588401
View online: http://dx.doi.org/10.1116/1.588401
View Table of Contents: http://scitation.aip.org/content/avs/journal/jvstb/14/2?ver=pdfcov
Published by the AVS: Science & Technology of Materials, Interfaces, and Processing

Articles you may be interested in

Thin-film growth of the charge-density-wave oxide Rb0.30MoO3
Appl. Phys. Lett. **68**, 3823 (1996); 10.1063/1.116629

Scanning tunneling spectroscopy on low- and high-T c superconductors
J. Vac. Sci. Technol. B **14**, 1224 (1996); 10.1116/1.588520

Spatial and energy variation of the local density of states in the charge density wave phase of 2H–NbSe2
J. Vac. Sci. Technol. B **14**, 1070 (1996); 10.1116/1.588402

Atomic force microscope and scanning tunneling microscope studies of superlattices and density waves in Fe doped NbSe2, TaSe2, TaS2 and in NbSe3 doped with Fe, Co, Cr, and V
J. Vac. Sci. Technol. B **12**, 1801 (1994); 10.1116/1.587603

Photothermal microscope for high-T c superconductors and charge density waves
Rev. Sci. Instrum. **64**, 3321 (1993); 10.1063/1.1144298

ADVERTISEMENT

Redistribution subject to AVS license or copyright; see http://scitation.aip.org/termsconditions. Download to IP: 128.103.96.231 On: Wed, 28 Oct 2015 19:48:08

Probing complex low-dimensional solids with scanning probe microscopes: From charge density waves to high-temperature superconductivity

Jie Liu, Jin-Lin Huang, and Charles M. Lieber
Department of Chemistry and Division of Applied Sciences, Harvard University, Cambridge, Massachusetts 02138

(Received 24 July 1995; accepted 1 December 1995)

Scanning probe microscopy (SPM) studies of low-dimensional solids have yielded significant advances in the understanding of collective phenomena in these complex materials. In this article, SPM studies from the authors' laboratory of charge density waves (CDWs) in metal dichalcogenide materials and of high-temperature copper–oxide superconductors (HTSCs) are reviewed. Temperature-dependent SPM studies of the structural properties of CDW phases in metal-doped tantalum disulfide (TaS_2) and tantalum diselenide ($TaSe_2$) have directly illuminated the problem of weak and strong CDW pinning. These studies have also led to the unexpected discovery of a hexatic CDW phase in niobium-doped TaS_2. SPMs have also been used to probe the structural and electronic properties of HTSCs. SPM studies of metal-doped $Bi_2Sr_2CaCu_2O_8$ (BSCCO) superconductors have been used to elucidate the complex crystal chemistry of this system. Comparisons of these data with electron diffraction measurements also highlight the importance of local crystallography in these complex materials. In addition, SPM studies have been used to elucidate the interaction of magnetic flux lines with surface defects, thus enabling a quantitative assessment of pinning by surface roughness. Finally, etching has been studied by *in situ* SPM and shown to be a promising means for controlling the properties of HTSC surfaces. © *1996 American Vacuum Society.*

I. INTRODUCTION

Understanding the relationships between structure, electronic properties, phase transitions, and observable properties in materials represents an important goal of condensed matter research.[1,2] Approaches to achieving this goal necessarily involve elucidating how material properties are determined by the arrangement of atoms and dopants on the atomic scale. In principle, this information is readily available from conventional diffraction and spectroscopy measurements when solids exhibit highly ordered, crystalline structures. However, some of the most fascinating solids known today, such as the high-temperature superconductors (HTSCs), are not well ordered. These complex materials exhibit structural complexities (e.g., substitutional disorder and/or incommensurate modulations) that conventional diffraction measurements cannot resolve. Experimental techniques that can probe material properties directly on the nanometer scale should thus afford researchers a unique opportunity to unravel these problems.

The ability of scanning probe microscopes (SPMs) to probe surface structure and electronic states on the atomic scale is now well recognized.[3] SPMs can also provide information essential to understanding bulk properties in many classes of materials.[2,4–7] In particular, solids that possess a large anisotropy in bonding—for example, strong covalent bonding in two-dimensional layers with weak noncovalent bonds holding these layers together—cleave preferentially along planes defined by the weak covalent bonds within the solid. The coordination of atoms at the surface cleavage plane in such anisotropic or low-dimensional solids is similar to that in the bulk, because the covalent bonding is unchanged. Hence, these cleaved surfaces usually do not reconstruct and their structure and electronic properties are thus representative of the bulk solid.

Highly anisotropic solids are amenable to SPM studies but, more importantly, these materials often exhibit scientifically fascinating structural and/or electronic phase transitions that represent one of the focal points of condensed matter research today. For example, a number of one- and two-dimensional transition metal chalcogenide materials are known to exhibit complex charge density wave (CDW) phases and, furthermore, it well known that the layered structure of the copper oxide materials is essential for high-temperature superconductivity. In this brief review, we will focus on our previous SPM studies of low-dimensional solids that have provided new information addressing important questions about CDWs and HTSCs. The implications of these results and ongoing studies will be discussed.

II. EXPERIMENT

An important issue in SPM investigations of low-dimensional solids is the preparation of suitable samples for analysis since most materials are not available commercially in single-crystal form. In general, our studies have focused on high-quality single crystals that are prepared and characterized by conventional techniques; these methods are briefly described below and have been discussed in more detail previously.[8–12]

Single crystals of transition metal dichalcogenides ($1T–TaS_2$ and $1T–TaSe_2$) and metal-doped transition metal dichalcogenides ($1T–Nb_xTa_{1-x}S_2$ and $1T–Ti_xTa_{1-x}Se_2$) were grown using iodine-vapor transport from prereacted

Redistribution subject to AVS license or copyright; see http://scitation.aip.org/termsconditions. Download to IP: 128.103.96.231 On: Wed, 28 Oct 2015 19:48:08

powders.[8–10] The prereacted powders and iodine were sealed in quartz tubes and placed in a two-zone furnace with the prereacted powders in the hotter zone. High-quality crystals were obtained after a three-week transport period using a ~70 °C temperature gradient. The metastable 1T crystal polytype is obtained by quenching the reaction tubes from their growth temperature. In all cases the crystal structure and composition was verified prior to SPM studies. In addition, the CDW phase transition temperatures were determined by temperature-dependent resistivity measurements. Single crystals of $Bi_2Sr_2CaCu_2O_8$(BSCCO-2212), $Bi_2Sr_2CuO_6$(BSCCO-2201), and Pb-doped BSCCO were grown from CuO-rich and/or Bi_2O_3-rich melts in MgO crucibles.[11,12] MgO crucibles are used by many research groups since they do not react extensively with the liquid phase and yield high-quality crystals with sharp transitions at $T_c \approx 90$ K.

In general, our SPM measurements have been made on cleaved single-crystal surfaces of the metal dichalcogenides and BSCCO superconductors. These materials can be cleaved readily using tape in air or ultrahigh vacuum (UHV). Several different instruments have been used to acquire the data discussed below. First, a number of the scanning tunneling microscopy (STM) studies were carried out in a N_2 filled glove box ($\leqslant$1 ppm H_2O and O_2) using commercial (Nanoscope, Digital Instrument, Inc.) and home-built electronics that controlled a microscope equipped with a variable temperature sample stage. More recent STM studies have been carried out using a low-temperature UHV microscope that can be operated at temperatures between 4.2 and 300 K. Finally, atomic force microscopy (AFM) studies have been carried out in air and in solution using a commercial instrument (Nanoscope III, Digital Instruments, Inc.) equipped with a fluid cell.

III. RESULTS AND DISCUSSION

A. Charge density waves

Prior to the discovery of STM, the structural properties of CDWs had been studies extensively using electron and x-ray diffraction.[13] While diffraction studies provided considerable insight into the basic structures of the CDWs in TaS_2 and $TaSe_2$, they were unable to elucidate clearly the structures of several of the complex incommensurate phases existing in TaS_2 and the effects of metal doping in these materials.[2,5] This situation changed significantly, however, following the demonstration by Coleman and co-workers that the charge modulation of a CDW could be viewed directly in real space.[14] The ability of STM to determine CDW and atomic lattice positions simultaneously was subsequently exploited by our group[2,5,7–10,15,16] and others[4,14,17,18] to resolve complicated structural details of incommensurate CDW phases in TaS_2, and to catalog the structures of CDW phases in a variety of transition metal dichalcogenide materials.[4]

Another general problem that STM has been especially useful in probing is how CDWs interact with metal impurities substitutionally doped in the atomic lattice. Understanding the nature of this interaction, called pinning, is essential to understanding the static and dynamic properties of the CDW state. In general, pinning can be defined as strong or weak. In strong pinning, the impurity potential dominates the CDW elastic energy and pins the phases of the CDW at each impurity site. In weak pinning, the CDW breaks up into constant phase regions that are pinned collectively by impurities.[7] Model investigations of weak and strong pinning by Nb and Ti impurities in $Nb_xTa_{1-x}S_2$ and $Ti_xTa_{1-x}Se_2$ are discussed below.

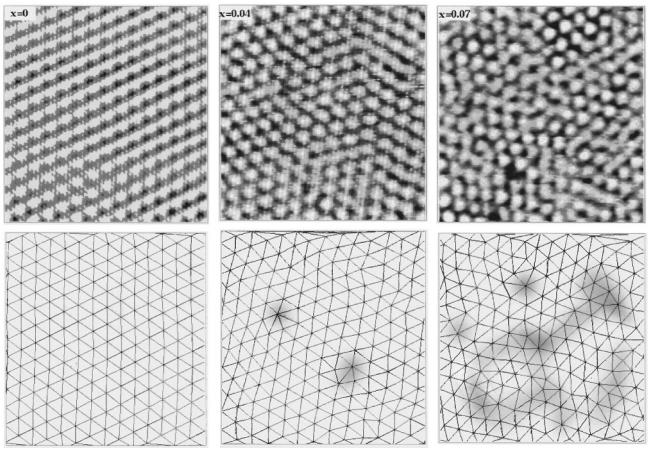

FIG. 1. STM images of the $Nb_xTa_{1-x}S_2$ crystals recorded at 380 ($x=0$), 340 ($x=0.04$), and 315 K ($x=0.07$). Delaunay triangulations are shown below each of the corresponding STM images. Topological defects in the triangulated images are highlighted with shading. Reproduced from Ref. 7.

Figure 1 shows STM images of $Nb_xTa_{1-x}S_2$ single crystals with values of x ranging from 0 to 0.07; the images were recorded at temperatures of 380 ($x=0$), 340 ($x=0.04$), and 315 K ($x=0.07$) in a glove box. These temperatures were chosen to ensure that the samples were in the incommensurate state where the CDW interacts only weakly with the underlying lattice.[10] Pure TaS_2 exhibits a regular hexagonal CDW lattice that is characteristic of the known incommensurate state in this material. As Nb atoms are substituted for Ta in the atomic lattice, the CDW lattice becomes less well ordered. The disorder in the CDW lattice appears to be due to the formation of dislocations and other topological defects. It is important to note, however, that the disorder does not appear to destroy the orientational order of the CDW lattice.[10] The presence of relatively long-range orientational order can be seen qualitatively by sighting down the rows of the CDW lattice: this shows that the average direction is defined regardless of the Nb impurity concentration.

To examine in more detail the topological defects and order of a lattice, it is instructive to carry out a Delaunay triangulation of the lattice sites.[16] This image analysis method, which is of general utility for any type of lattice, has been applied previously by several groups.[19] The triangulation uniquely defines the nearest neighbors and thus the coordination number of each CDW maxima; in the triangulation, nearest neighbors are connected by ''bonds'' with vertices corresponding to the CDW maxima. Fully coordinated lattice sites have six bonds, while topological defects containing fewer or greater than six bonds are highlighted by

Redistribution subject to AVS license or copyright; see http://scitation.aip.org/termsconditions. Download to IP: 128.103.96.231 On: Wed, 28 Oct 2015 19:48:08

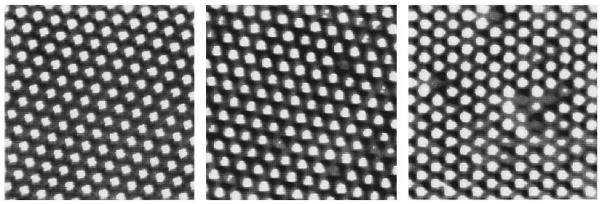

FIG. 2. The 13.5×13.5 nm^2 STM images of $TaSe_2$ (left), $Ti_{0.02}Ta_{0.98}Se_2$ (middle), and $Ti_{0.04}Ta_{0.96}Se_2$ (right) samples recorded at room temperature. The bright yellow features in these images correspond to the CDW maxima. Reproduced from Ref. 9.

shading. The triangulated images are shown below their corresponding STM images in Fig. 1. These data demonstrate clearly that the pure 1T–TaS_2 CDW lattice is defect free, and that the number of topological defects increases with increasing Nb impurity concentration. Significantly, analysis of the average topological defect spacing shows that it is much greater than the average spacing between Nb impurities, and thus this analysis unambiguously shows that the pinning by Nb atoms is a weak or collective effect.[16]

It is also possible to further characterize the order in this system by calculating the translational, $G_T(\mathbf{r})$, and orientational, $G_6(\mathbf{r})$, correlation functions.[7,16] Analyses of $G_T(\mathbf{r})$ and $G_6(\mathbf{r})$ as a function of the Nb impurity concentration show that (1) for $x=0$ both $G_T(\mathbf{r})$ and $G_6(\mathbf{r})$ exhibit long-range order, (2) for $0<\times\leqslant 0.04$ $G_T(\mathbf{r})$ decays exponentially (i.e., shows short-range order) and $G_6(\mathbf{r})$ exhibits long-range order, and (3) for $x\geqslant 0.07$ $G_T(\mathbf{r})$ and $G_6(\mathbf{r})$ decay exponentially. The existence of long-range orientational order but short-range translational order is an important observation because it strongly suggests the existence of a hexatic glass state in these doped materials. Hence, these studies were able to show that the CDW lattice evolves from a crystalline state in the pure solid through a hexatic glass state to a liquidlike amorphous state as the impurity concentration increases.

A very different impurity pinning effect has been observed in our STM studies of Ti-doped $TaSe_2$.[9] The CDW state in 1T–$TaSe_2$ is commensurate at all experimentally accessible temperatures. In the commensurate CDW state, each CDW maximum is located on the same symmetric Ta atom site; that is the CDW is effectively pinned to the underlying atomic lattice. The driving force for the commensurate state is an electrostatic interaction between the Ta ions and the CDW. In the incommensurate state, this electrostatic pinning term is zero. The strong interaction between the CDW and atomic lattice in the commensurate state suggests that the effect of metal impurities should be quite distinct from that observed in the $Nb_xTa_{1-x}S_2$ materials. STM images recorded on a series of $Ti_xTa_{1-x}Se_2$ single crystals with $x=0$, 0.02 and 0.04 support this idea (see Fig. 2). The CDW lattices observed in samples containing Ti impurities exhibit a regular hexagonal structure that is similar to the pure sample, and are thus very different than observed in the $Nb_xTa_{1-x}S_2$ materials. The images of the Ti-doped materials also exhibit localized regions where the CDW amplitude is suppressed relative to the surrounding CDW maxima. In addition, we have

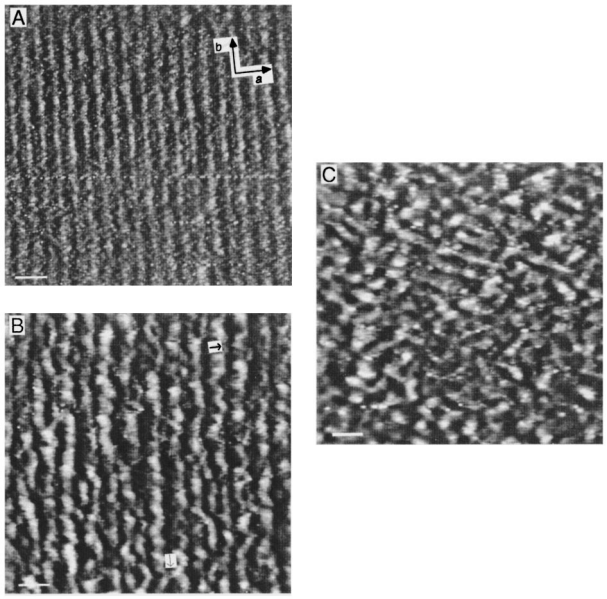

FIG. 3. STM images of (A) $Bi_2Sr_2CaCu_2O_8$, (B) $Pb_{0.3}Bi_{1.7}Sr_2CaCu_2O_8$, and (C) $Pb_{0.5}Bi_{1.5}Sr_2CaCu_2O_8$. The underlying **a–b** cell axes are indicated in (A). The white bar corresponds to 5 nm in these images. Reproduced from Ref. 11.

shown that the density of these localized defects increases linearly with the Ti impurity concentration. These data and the highly localized nature of the CDW defects represent solid evidence for strong pinning. Hence, real-space STM studies of $Nb_xTa_{1-x}S_2$ and $Ti_xTa_{1-x}Se_2$ materials have provided a solid structural picture of the concepts of weak and strong pinning in CDW materials.

B. Copper oxide superconductors

There have also been a number of SPM studies reported in the literature that address the structure and electronic properties of HTSC materials.[2,6,20,21] Herein, we focus primarily on work from our laboratory that has addressed (1) the local crystal chemistry and doping, (2) the role of structural defects in pinning magnetic flux lines, and (3) the control of surface morphology by chemical etching.

We have performed extensive studies of the structural effects of metal substitution in the HTSC materials.[6,11,21,23] A particularly informative example of these studies is the case of Pb-doped BSCCO where we have characterized the structural consequences of Pb substitution for Bi in both 2212 and 2201 crystal types. STM images of the Bi(Pb)–O layer of Pb-doped BSCCO-2212 single crystals are shown in Fig. 3.[22] Images of pure ($x=0$) BSCCO-2212 crystals exhibit a one-dimensional, incommensurate superstructure that is characteristic of the BSCCO materials.[11] As Pb is substituted for Bi in these crystals, however, the superstructure exhibits increasing disorder. The one-dimensional superstructure is still clear at low Pb concentrations ($\times\leqslant 0.2$), although there are obvious distortions such as variations in the period from 25 to 39 Å. At higher Pb concentration we found that there was little periodicity at length scales expected for the superstruc-

Redistribution subject to AVS license or copyright; see http://scitation.aip.org/termsconditions. Download to IP: 128.103.96.231 On: Wed, 28 Oct 2015 19:48:08

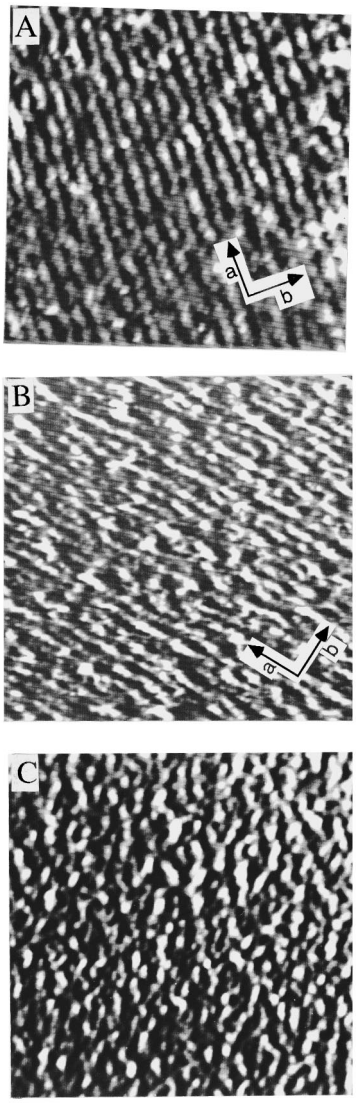

FIG. 4. The 60×60 nm^2 images of (A) $Bi_2Sr_2CuO_6$, (B) $Pb_{0.15}Bi_{1.85}Sr_2CuO_6$, and (C) $Pb_{0.3}Bi_{1.7}Sr_2CuO_6$.

ture, and thus it is apparent that Pb-induced disorder ultimately destroys this one-dimensional superlattice. These large structural changes also can have important implications for superconductivity. In particular, we have shown that the superconducting critical current density (J_c) increases significantly with Pb doping in BSCCO-2212.[24] This increase in J_c is believed to arise from enhanced flux-line pinning by the structural disorder caused by Pb substitution.

We have also carried out similar studies on Pb-substituted BSCCO-2201 crystals. In general, the STM images of the Pb-doped 2201 crystals were similar to those obtained on the Pb-doped 2212 crystals; that is, increasing disorder was observed as the Pb concentration was increased (see Fig. 4). To quantify the order in these crystals to compare our results to those obtained by electron diffraction we have also calculated the two-dimensional structure factor $S_{2D}(\mathbf{k})=|\rho(\mathbf{k})|^2$, where $\rho(\mathbf{k})$ is the Fourier transform of the atom density, from images as a function of Pb concentration. Consideration of this analysis suggests at least two significant points. First, at intermediate Pb concentrations our comparison of $S_{2D}(\mathbf{k})$ with in-plane electron diffraction patterns shows that the multiple superlattices inferred from electron diffraction are due to harmonics of the fundamental superlattice period. Second, at higher Pb concentrations this same comparison demonstrates that the absence of a superlattice in electron diffraction patterns is due to the extreme disorder of the structural modulation; that is, the crystal is not well ordered. More generally, this approach of calculating $S_{2D}(\mathbf{k})$ from real-space images enables the quantitative determination of local crystalline order, and thus will be complementary to conventional diffraction techniques in elucidating microstructure of complex materials.

The surface defects described above as well as bulk defects can play an important role in pinning magnetic flux lines in HTSC materials.[25] Because flux-line pinning determines to a large extent the magnitude of J_c in superconductors (and therefore possible applications), an understanding of pinning is central to much work in the HTSC field. Several techniques, including Bitter decoration and neutron diffraction, have been used to study the structure of flux-line lattices. While both of these techniques have provided significant insight into the structure of flux-line lattices, they have not been able to provide direct information about defects that pin the flux lines. STM and magnetic force microscopy are capable of imaging both flux lines and crystal structure (defects) simultaneously, and recent results suggest that these promising techniques will play an increasingly important role in the future.[26,27]

Alternatively, a new approach that we have developed combining conventional Bitter decoration and AFM has yielded significant insight into the structure and pinning of magnetic flux lines.[28] Bitter decoration provides a well-established technique for highlighting reproducibly large numbers of flux lines and, when combined with AFM, enables us to image the decorated flux-line positions and map out surface defects with nanometer scale resolution. Typical AFM images obtained on BSCCO single crystals that had been decorated in a magnetic field of 33 G are shown in Fig. 5. Two distinct types of structures are seen in these images: the magnetic flux-line positions, which appear as small circular spots, and surface steps. Analysis of the surface topography demonstrates that these steps have heights of 30, 100, and 300 nm, respectively. More important, we have shown that the flux-line lattice structure can differ significantly depending on the surface step height.[28]

The flux-line lattice orientation is seen most clearly in two-dimensional Fourier transform (2DFT) power spectra of selected regions of these images. In Fig. 5(A), the flux-line lattice orientation is independent of surface step as is clearly evident when comparing the flux-line lattice reciprocal lattice vectors with the step direction. In Fig. 5(B) which contains a larger step, the 2DFT shows that a principle axis of the flux-line lattice is aligned preferentially along the straight section of the step. The overall orientation of the flux-line lattice is not perturbed, however, by the curvature in the step at the bottom of the image. The structure of the flux-line

Redistribution subject to AVS license or copyright; see http://scitation.aip.org/termsconditions. Download to IP: 128.103.96.231 On: Wed, 28 Oct 2015 19:48:08

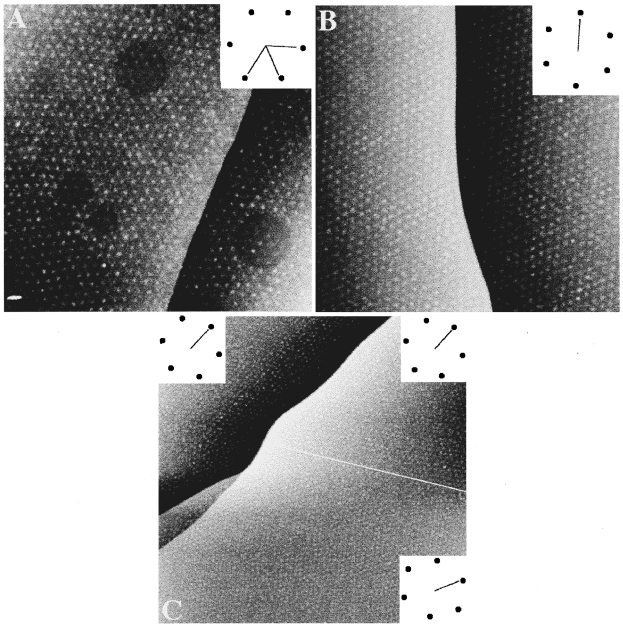

FIG. 5. AFM images recorded on a BSCCO crystal that was decorated at 4.2 K in a magnetic field of 33 G. Each image shows a surface step that crosses the crystal surface. The insets correspond to 2DFTs calculated from the AFM images; the 2DFTs have been rotated by 90° so that the reciprocal lattice vectors can be compared directly with the real-space directions. In (A) and (B) the 2DFTs were calculated from the entire images; in (C) the three 2DFTs were calculated from the areas of the image where they are displayed. The images in (A), (B), and (C) are 25.4, 31.5, and 49.6 μm on a side, respectively. Reproduced from Ref. 28.

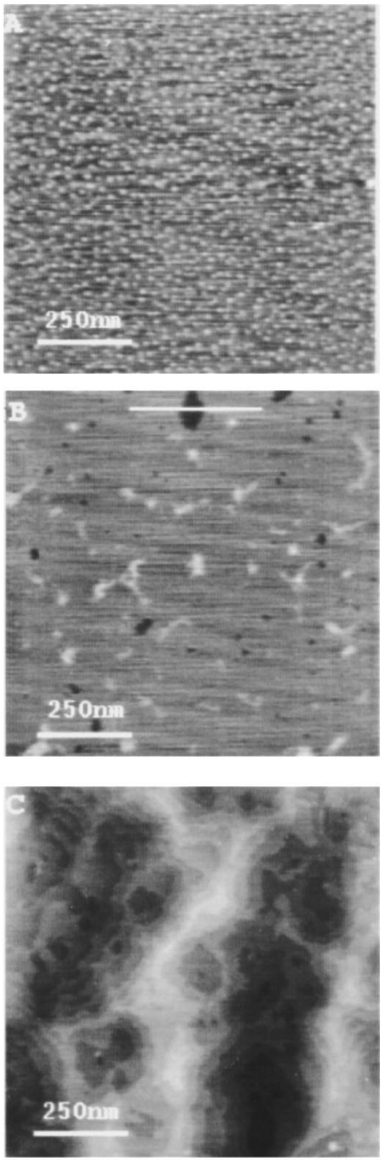

FIG. 6. AFM images of a BSCCO crystal recorded (A) before etching, (B) after etching with a dilute bromine solution, and (C) after etching with a concentrated bromine solution. The step heights in images (B,C) are ~1.5 nm.

lattice in Fig. 5(C), which contains the largest step, is more complex and interesting. In the upper left of the image the 2DFT shows that the flux-line lattice orientation is pinned to the step direction. The flux-line lattice in the upper right portion of the image is also pinned in this same orientation. However, the 2DFT demonstrates that the flux-line lattice orientation in the lower right part of the image is rotated relative to the upper part. This rotation follows the change in step direction that occurs at the bottom of the image. Significantly, the two distinct flux-line lattice orientations lead to the formation of a grain boundary in the lattice. We have developed a model to understand the propagation of these grain boundaries by considering the pinning energy associated with the surface step and the energy to elastically deform the flux lattice.[25] More important, using the AFM data has made it possible to demonstrate that the grain boundaries propagate completely through the superconductor samples and thus influence significantly the bulk structure of the flux-line lattice.

The complex surface properties of the HTSCs described above have also led to difficulties in making reliable STM spectroscopy measurements and in fabricating controlled junctions needed for applications. These problems arising from the complex surface properties of HTSC materials can in principle be overcome by either (1) a controlled removal of specific oxide layers via etching,[29] or (2) through selective termination of thin-film growth with a particular oxide layer.[30] We have recently begun systematic studies of the etching approach using force microscopy. The emphasis in this work is to exploit specific chemical etchants to control the surface morphology of these complex materials. For example, we have investigated the solvent and concentration dependence of bromine/alcohol etching of BSCCO surfaces and found that it is possible to vary the etching process from layer by layer to nearly vertical (see Fig. 6). Figure 6(B) shows an atomically flat BSCCO surface obtained by layer-by-layer etching; the surface features in this image all correspond to half unit cell steps of ~1.5 nm. In contrast, Fig. 6(C) shows that higher etchant concentrations produce primarily vertical etching of the BSCCO surface. To demonstrate the generality of this technique we have also carried out similar studies on $La_{1.8}Sr_{0.2}CuO_4$ (LSCO) crystals. The step-terrace structure exhibited in Fig. 7 shows that it is pos-

Redistribution subject to AVS license or copyright; see http://scitation.aip.org/termsconditions. Download to IP: 128.103.96.231 On: Wed, 28 Oct 2015 19:48:08

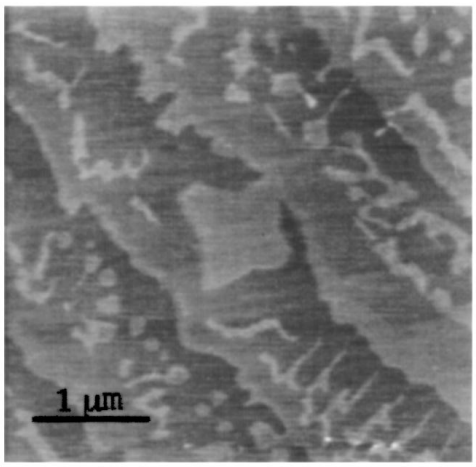

FIG. 7. AFM image of a LSCO single crystal surface etched with a bromine solution. The step heights in this image are ~0.7 nm.

sible to obtain layer-by-layer etching with this system as well. We believe that the ability to control the etching from layer-by-layer to vertical will have significant implications in fabrication steps such as planarization and pattern definition.

IV. CONCLUSIONS

In summary, we have reviewed SPM studies from our laboratory that have focused on low-dimensional materials exhibiting CDWs and HTSC. Temperature-dependent SPM studies of the structural properties of CDW phases in metal-doped TaS_2 and $TaSe_2$ have provided a much deeper understanding of weak and strong CDW pinning, and have led to the discovery of a hexatic CDW phase in niobium-doped TaS_2. STM studies of metal-doped BSCCO 2212 and 2201 superconductors have been used to elucidate the complex crystal chemistry of this system. These studies have provided a clear explanation for enhanced critical currents in Pb-doped materials, and highlight the general potential of local crystallography for unraveling complex materials problems. A new approach combining AFM and decoration has also been developed and used to elucidate the interaction of magnetic flux lines with surface defects, thus enabling the first quantitative assessment of pinning by surface roughness. Finally, etching has been studied by *in situ* SPM and shown to be a promising means for controlling the structure and electronic properties of HTSC surfaces.

[1]*Physics Through the 1990s: Condensed-Matter Physics* (National Academy of Sciences, Washington, DC, 1986).
[2]C. M. Lieber, Chem. Eng. News **18**, 28 (1994).
[3]See, for example: *Scanning Tunneling Microscopy*, edited by J. A. Stroscio and W. J. Kaiser (Academic, New York, 1993).
[4]R. V. Coleman, B. Giambattista, P. K. Hansma, A. Johnson, W. W. McNairy, and C. G. Slough, Adv. Phys. **37**, 559 (1988).
[5]C. M. Lieber and X. L. Wu, Acc. Chem. Res. **24**, 170 (1991).
[6]Z. Zhang and C. M. Lieber, J. Phys. Chem. **96**, 2030 (1992).
[7]H. Dai and C. M. Lieber, Annu. Rev. Phys. Chem. **44**, 237 (1993).
[8]H. Chen, X. L. Wu, and C. M. Lieber, J. Am. Chem. Soc. **112**, 3326 (1990).
[9]X. L. Wu and C. M. Lieber, Phys. Rev. B **41**, 1239 (1990).
[10]H. Dai, H. Chen, and C. M. Lieber, Phys. Rev. Lett. **66**, 3183 (1991).
[11]X. L. Wu, Z. Zhang, Y. Wang, and C. M. Lieber, Science **248**, 1211 (1990).
[12]Y. Li, J. Liu, and C. M. Lieber, Phys. Rev. B **49**, 6234 (1994).
[13]J. A. Wilson, F. J. DiSalvo, and S. Mathajan, Adv. Phys. **24**, 117 (1975); R. L. Withers and J. A. Wilson, J. Phys. C **19**, 4809 (1986).
[14]R. V. Coleman, B. Drake, P. K. Hansma, and G. Slough, Phys. Rev. Lett. **55**, 394 (1985).
[15]X. L. Wu and C. M. Lieber, Science **243**, 1703 (1989); X. L. Wu and C. M. Lieber, Phys. Rev. Lett. **64**, 1150 (1990).
[16]H. Dai and C. M. Lieber, Phys. Rev. Lett. **69**, 1576 (1992).
[17]R. E. Thomson, U. Walter, E. Ganz, J. Clarke, A. Zettl, P. Rauch, and F. J. DiSalvo, Phys. Rev. B **38**, 10734 (1988); B. Giambattista, C. G. Slough, W. W. McNairy, and R. V. Coleman, *ibid*. **41**, 10082 (1990).
[18]G. Gammie, J. S. Hubacek, S. L. Skala, R. T. Brokenbrough, J. R. Tucker, and J. W. Lyding, Phys. Rev. B **40**, 9529 (1989); C. G. Slough and R. V. Coleman, *ibid*. **40**, 8042 (1989).
[19]D. R. Nelson, M. Rubinstein, and F. Spaepen, Philos. Mag. A **46**, 105 (1982); C. A. Murray, W. O. Sprenger, and R. A. Wenk, Phys. Rev. B **42**, 688 (1991).
[20]J. R. Kirtley, Int. J. Mod. Phys. B **4**, 201 (1990).
[21]Z. Zhang and C. M. Lieber, in *Materials Chemistry: An Emerging Discipline*, edited by L. V. Interrante, L. A. Casper, and A. B. Ellis (American Chemical Society, Washington, DC, 1995), p. 480.
[22]Z. Zhang, Y. L. Wang, X. L. Wu, J. L. Huang, and C. M. Lieber, Phys. Rev. B **42**, 1082 (1990).
[23]Z. Zhang, C. C. Chen, C. M. Lieber, B. Morosin, E. L. Venturini, and D. S. Ginley, Phys. Rev. B **45**, 987 (1992).
[24]Y. L. Wang, X. L. Wu, C. C. Chen, and C. M. Lieber, Proc. Natl. Acad. Sci. U.S.A. **87**, 7058 (1990).
[25]H. Dai, J. Liu, and C. M. Lieber, Phys. Rev. Lett. **72**, 748 (1994).
[26]H. F. Hess, C. A. Murray, and J. V. Waszczak, Phys. Rev. B **50**, 16528 (1994).
[27]A. Moser, H. J. Hug, I. Parashikov, B. Stiefel, O. Fritz, H. Thomas, A. Baratoff, H.-J. Guntherodt, and P. Chaudhari, Phys. Rev. Lett. **74**, 1847 (1995).
[28]S. Yoon, H. Dai, J. Liu, and C. M. Lieber, Science **265**, 215 (1994).
[29]J. M. Valles, Jr., R. C. Dynes, A. M. Cucolo, M. Gurivitch, L. F. Schneemeyer, J. P. Garno, and J. V. Waszczak, Phys. Rev. B **44**, 11986 (1991).
[30]K. Koguchi, T. Matsumoto, and T. Kawai, Science **267**, 71 (1994).

Redistribution subject to AVS license or copyright; see http://scitation.aip.org/termsconditions. Download to IP: 128.103.96.231 On: Wed, 28 Oct 2015 19:48:08